# Assessment of Tissue Viability Following Electroosmotic Push–Pull Perfusion from Organotypic Hippocampal Slice Cultures

Amy E. Rupert,[†] Y. Ou,[†] M. Sandberg,[‡] and S. G. Weber*[,†]

[†]Department of Chemistry, University of Pittsburgh, Pittsburgh Pennsylvania 15260, United States
[‡]Department of Medical Biochemistry and Cell Biology, Gothenburg University, Gothenburg, S 405 30 Sweden

S *Supporting Information*

ABSTRACT: We have developed a novel sampling technique that allows both introduction and removal of fluid from the extracellular space of living tissue. This method is based on the fluidics of push–pull perfusion but flow is driven by electroosmosis. We have applied this method to organotypic hippocampal cultures. A source capillary is inserted into the tissue and a collection capillary is in contact with the tissue surface through a thin layer of fluid. A voltage is applied across the proximal ends of source and collection capillary. In the applied field, fluid will move from source, into the tissue, and then be collected. In this process, damage to cells may occur. To understand better what sampling conditions influence damage most, we tested various sampling geometries and applied voltages, quantifying damage 16–24 h later using propidium iodide as a cell death marker. We found that damage correlates with both voltage drop and power dissipated in the tissue, but that voltage drop is a better indicator of damage when comparing models in which capillary arrangement and length are different.

KEYWORDS: Organotypic hippocampal cultures, sampling, electroosmosis, injury, push–pull perfusion
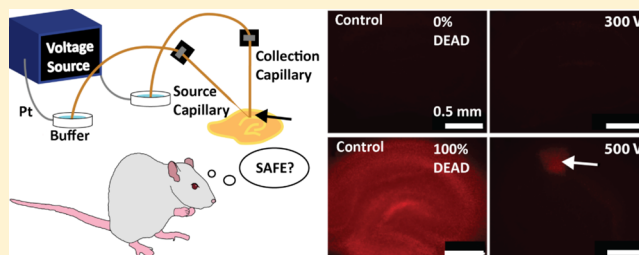
The efficacy of a chemical signal in the brain depends on its ability to reach a target receptor. The journey of a neurotransmitter or neuromodulator to a target receptor is especially treacherous during volume transmission. As it makes its way through the extracellular fluid, the neuroactive molecule may diffuse away from its target receptor, be removed from the extracellular fluid by uptake, or be degraded or modified by extracellular enzymes. Neuropeptides are hydrolyzed by ectopeptidases—membrane-bound, outward facing enzymes. Thus, modulation of an effect of a neuropeptide can be governed by the location and activity of ectopeptidases. We are interested in this process, particularly in endogenous ectopeptidase activity that degrades galanin, a 29-amino acid, C-terminal amidated peptide (30 with a carboxylate C-terminus in humans) that is neuroprotective against excitotoxicity both in vitro[1−3] and in models of seizure in vivo.[4−6] Galanin-like immunoreactivity increases in the postischemic gerbil hippocampus in vivo.[7] In response to ischemic injury, the brain may foster neuroprotection through galaninergic pathways by increasing release to the extracellular space or decreasing degradation. In both cases, the likelihood of galanin reaching, binding to, and activating the galanin receptor would be greater.

One way to investigate the dynamics of ectopeptidases activity is to expose ectopeptidases to substrate and measure the product of the enzymatic reaction in a time-dependent manner. A typical determination of ectoenzymatic activity in tissue involves isolation of the membrane fraction from a tissue homogenate prepared from a known weight of tissue followed by determination of the rate of substrate conversion to product.[8−12] A more informative approach would involve introduction of substrate to the extracellular space of intact brain tissue for a known amount of time followed by analysis of the contents of the extracellular space after a given time. Microdialysis has been used to study enzymatic reactions, but the dialysis membrane limits the size of what can be introduced or recovered.[13−22] In addition, the spatial resolution of microdialysis may also be a limitation. Low-flow (LF) push–pull perfusion,[23−25] while it has not been used to study enzyme reactions, can in principle both directly introduce a substrate to the extracellular fluid with subsequent removal of products from tissue. The LF push–pull cannula consists of concentric or adjacent capillary tubes and uses pressure-driven flow to push fluid through the center capillary into a sample while a vacuum is applied to the outer capillary to remove perfused fluid from the tissue. Flow rates ranging from 1 to 50 nL/min are achievable, rates that minimize damage and, in the lower region (1–2 nL/min), sample slowly enough so as not to remove fluid faster than it can be replenished.[23,26,27] However, a careful balance of pressure and vacuum must be maintained to regulate this flow, and once in the tissue sample the direction and velocity of the fluid is no longer directly controlled.
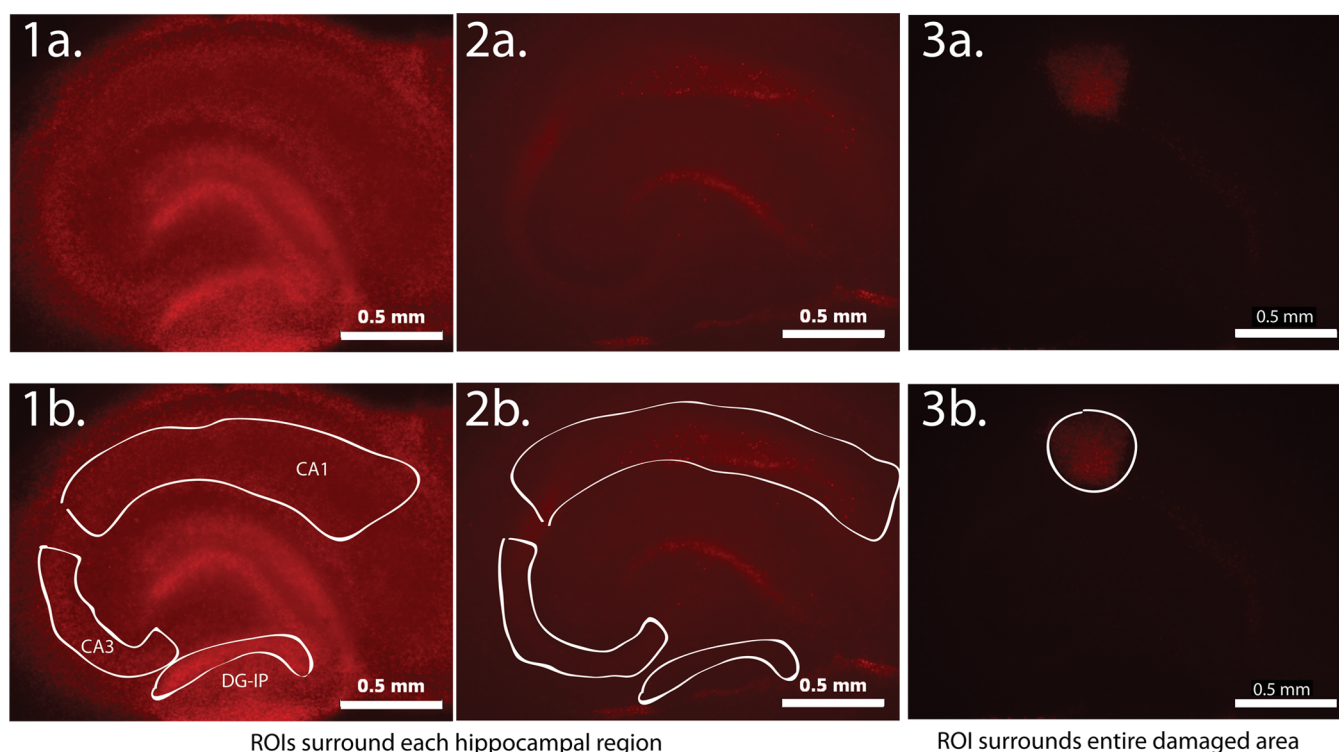
Figure 1. Representative images of tissues stained with PI following EOPPP and ROIs for quantitation. Scale bar = 0.5 mm. (1a) MeOH-treated positive control tissue with (1b) regional ROIs drawn around the Cornu Ammonis region 1 (CA1), Cornu Ammonis region 3 (CA3), and infrapyramidal blade of the dentate gyrus (DG-IP). (2a) Negative control tissue with (2b) regional ROIs drawn around the CA1, CA3, and DG-IP. (3a) Sampled tissue with damage in CA1 region and (3b) "local" ROI drawn around the PI fluorescence. The contrast in the negative control image (2a and 2b) has been increased to facilitate visualization of the hippocampal structure.

We have developed a method that is, in some ways, similar to low-flow push–pull perfusion. This new method, termed electroosmotic push–pull perfusion (EOPPP), employs two capillaries. An applied current passes from one capillary, through the tissue, into the other capillary. Fluid moves in the same path and direction by electroosmotic flow.[28] A primary concern when investigating living brain tissue with invasive probes is disruption of the neurochemistry that we seek to understand. Considerations of sample-site disruption are reflected in the history of sampling development; microdialysis was developed in the 1980s to avoid perturbations from early push–pull perfusion methods.[29−31] Recently developed low-flow push–pull perfusion uses flow rates in the nanoliters per minute range[23,27] which causes minimal damage to cells in the rat retina in vivo. Even in microdialysis, while many suggest that an equilibration period of 24−48 h after probe implantation is sufficient to allow surrounding tissue to recover from surgical procedures,[32] evidence shows that implantation of the probe alters intrinsic neurochemistry and that the measurements may suffer from reduced sensitivity to analyte in the extracellular space due to an immune response and astrogliosis.[33,34] These effects must be understood and taken into account to understand properly the information derived from collected samples.[35,36] To assess the extent of damage from EOPPP, we used propidium iodide (PI) as a cell death marker.[37] We also couple experimental investigations with finite element modeling to determine what aspects of the sampling geometry or conditions influence damage the most with the goal of defining conditions that minimize damage.

RESULTS AND DISCUSSION

Quantifying Damage. To quantify damage, images of PI-stained sampled tissues were quantitatively compared to images of PI-stained positive controls (PC) and negative controls (NC).

PI fluorescence in regions of interest (ROIs) was measured using SimplePCI software. ROIs were drawn where there was visible damage. An ROI was also created around each hippocampal region in both positive and negative controls, as shown in bottom panels of Figure 1 (1b, 2b, and 3b). We measured the mean fluorescence intensity (I_f) and area of each ROI. For accurate delineation of ROIs, we increased the image contrast. Unmodified images were used for quantifying cell death in the image.

The damage in the sampled region (i.e., Cornu Ammonis Area 3, CA3) was calculated using eq 1 where I is fluorescence intensity and subscripts S and NC refer to sampled and negative control, respectively. A_R is the area of the particular region where sampling occurred.

$$\text{damage in sampled tissue} = (I_S - I_{NC})A_R \qquad (1)$$

This represents sampling-induced PI fluorescence, which we will refer to as "damage". This value was then used to calculate the fraction of susceptible cells in the sampled region (e.g., CA3) by using the damage found in the positive control, eq 2, as a reference. This calculation was important when comparing damage between different sized regions. The damage for each region in positive control is (mean ± standard error of the mean (SEM)) 23.3 ± 1.2, 43.6 ± 4.0, and 8.2 ± 4.8 for the CA3, Cornu Ammonis area 1 (CA1), and infrapyramidal blade
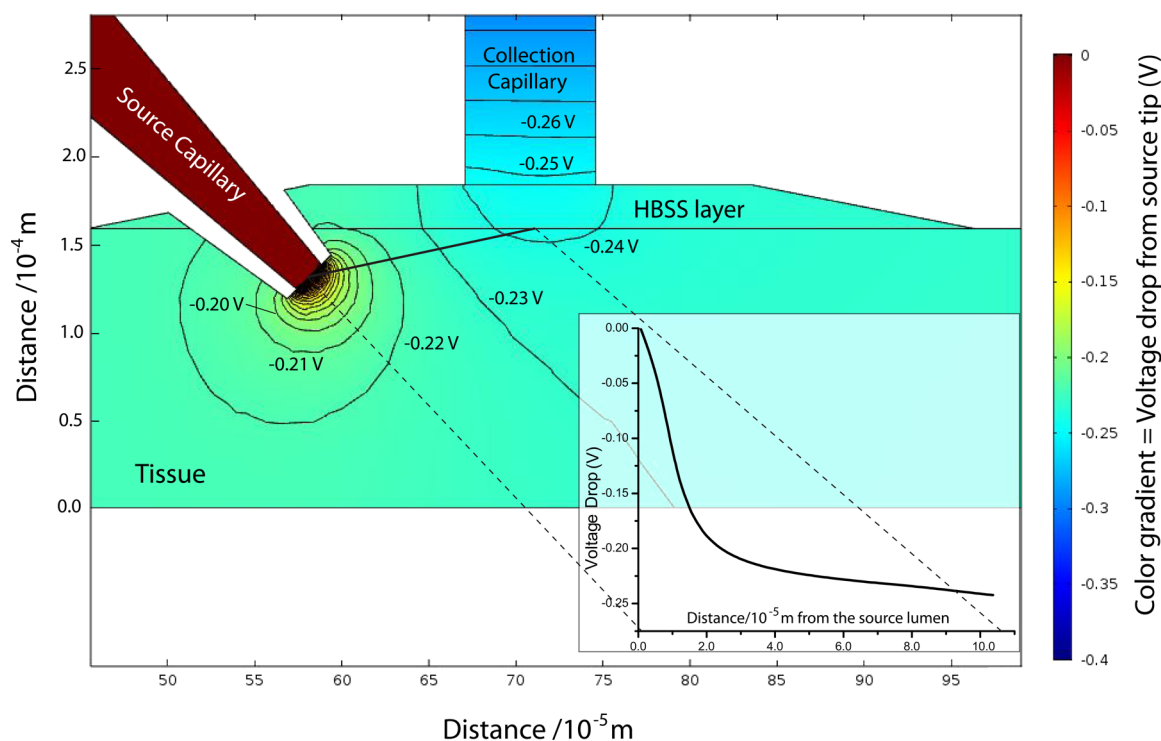
Figure 2. Surface/contour color plot of the voltage drop from source tip. The plane shown contains the symmetry axes of the two capillaries and zooms in on the area between them. A voltage difference of 300 V was applied across two 30 cm long capillaries: a 200 μm source capillary pulled to a 20 μm tip inserted 40 μm into the tissue was at 0 V and a 75 μm collection capillary 25 μm above the surface (contacting the tissue by a layer of HBSS) of the tissue is held at −300 V. The color gradient indicates voltage drop. Contour lines accompany the surface color plot, and are labeled with the corresponding voltage drop from the center of the source capillary lumen. Inset is a plot of voltage drop along the line that connects the source capillary tip lumen to the tissue surface under the center of the collection capillary.

of the dentate gyrus (DG-IP), respectively. These values have units of fluorescence intensity.

$$\text{damage in positive control} = (I_{PC} - I_{NC})A_R \qquad (2)$$

Finite Element Modeling. In single capillary electro-osmotic sampling,[38,39] a correlation was found between the power dissipated within the tissue and the damage induced by the sampling.[40] In that analysis, power was calculated by multiplying the experimental current by the voltage drop within the tissue. This voltage drop was calculated numerically in COMSOL Multiphysics, a finite elements modeling program. We began with a similar approach for EOPPP, using COMSOL to calculate the power and voltage drop within the tissue when a potential difference is applied to the ends of the source and collection capillaries. In a recent report,[40] we oversimplified our treatment of tissue conductivity. In that report, the tissue conductivity was calculated as the bulk electrolyte conductivity multiplied by the porosity, ε (0.41[41]). In reality, tissue conductivity scales as a factor that includes both porosity and tortuosity often called the formation factor in the geology literature.[42] In models of porous media, this factor is often given as ε/λ^2 (where λ is the geometric tortuosity of the porous material).[43] While there is no report of a geometric tortuosity for OHSC tissues prepared from early postnatal rats, we use the best approximation, 1.39, obtained by electrochemical measurements of the diffusion of TMA in p5-p7 *acute* hippocampal slices.[41] EOPPP was modeled in a 3D workspace in COMSOL Multiphysics (v. 4.3). Figure SI-1 in the Supporting Information lists boundary conditions and subdomain properties and contains a screenshot of the model in the COMSOL workspace. We also remodeled single capillary electroosmotic

sampling, with the appropriate treatment of conductivity. Figure SI-2 is a sketch of the single capillary model with relevant boundary and subdomain conditions. Numerical solutions of the Laplace equation were used to calculate the voltage drop within the tissue. Figure 2 is a color surface plot with contour labels of the voltage drop in a tissue being sampled.

We first focused on damage trends as they may relate to the voltage drop in the tissue. To calculate voltage drop, we modeled various sampling geometries in COMSOL and found the difference in voltage between the middle of the source lumen and the tissue under the center of the collection lumen. Four geometrical parameters were varied to investigate damage trends: source tip diameter, source insertion depth, collection capillary diameter, and collection capillary-to-tissue distance. To get a better idea of which parameters actually contribute to voltage drop, one variable was changed at a time to see the effect of that particular variable. Figure 3 illustrates the effect of changing different components of the sampling geometry on voltage drop. As voltage drop scales directly with applied voltage, the ratio of voltage drop to applied voltage (V_{tissue}/V_{app}) is calculated on the y-axis. One geometry was chosen as a reference point (200 μm source barrel, 20 μm source tip inserted 40 μm into the tissue, and a 75 μm collection capillary 25 μm above the tissue surface), and the effects of changing each component to a larger or smaller dimension was investigated.

Simplified Calculations of Voltage Drop. The voltage drop in the tissue was estimated without the use of COMSOL by simply calculating the tissue's resistance compared to the
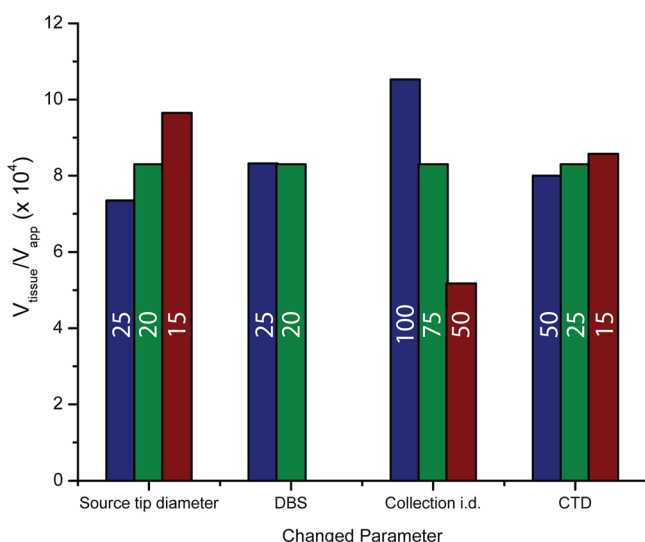
Figure 3. Effect of changing sampling geometry on the average electric field in the tissue. The green bar in each case corresponds to 200 μm source i.d. with a 20 μm tip inserted 40 μm into the tissue (DBS) and a 75 μm collection i.d. with a capillary-to-tissue distance (CTD) of 25 μm. The blue and red bars represent increasing or decreasing the indicated parameter to the size listed on the bar (listed in μm).

resistance of the entire system. Figure 4 is a sketch of the sampling system, simplified as resistors in series.
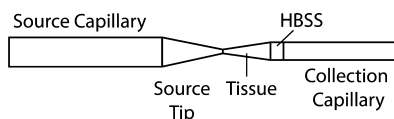
Figure 4. Simple resistance model for calculating voltage drop across the tissue. The source capillary, collection capillary, and the layer of HBSS between tissue and collection lumen are represented as cylindrical resistors. We treat the source tip and tissue as truncated cones.

To calculate the values shown in Figure 4, we first started by calculating the resistance (R) of each component (eqs 3−7).

$$R_{\text{sourcecapillary}} = \frac{1}{\sigma} \frac{l_{\text{sourcecapillary}}}{\pi r_{\text{sourcecapillary}}^2} \quad (3)$$

$$R_{\text{sourcetip}} = \frac{1}{\sigma} \frac{l_{\text{sourcetip}}}{\pi r_{\text{sourcecapillary}} r_{\text{sourcetip}}} \quad (4)$$

$$R_{\text{tissue}} = \beta \frac{\lambda^2}{\sigma \varepsilon} \frac{l_{\text{tissue}}}{\pi r_{\text{sourcetip}} r_{\text{collectioncapillary}}} \quad (5)$$

$$R_{\text{HBSS}} = \frac{\text{CTD}}{\pi \sigma r_{\text{ODcollectioncapillary}}^2} \quad (6)$$

$$R_{\text{collectioncapillary}} = \frac{1}{\sigma} \frac{l_{\text{collectioncapillary}}}{\pi r_{\text{collectioncapillary}}^2} \quad (7)$$

Sigma (σ) is the conductivity of the electrolyte filling the capillaries, r or l specifies the radius or length, respectively, of the component in subscript. In eq 5, the factor λ^2/ε is the inverse of the formation factor. The "length" of the tissue was calculated using the geometry in Figure SI-3. We approximated

the source tip and the tissue as truncated cones. β corrects for our approximation that the tissue in this model is cone-shaped spanning from the source lumen to an imaginary boundary the shape of and directly underneath the collection lumen on the tissue surface; in reality, current is not restricted to a cone. CTD is the collection capillary-to-tissue distance, and the radius in the denominator of eq 6 is the radius of the outer diameter of the capillary wall. Equation 8 estimates the portion of the total voltage that occurs in the tissue.

$$V_{\text{tissue}}/V_{\text{app}} = R_{\text{tissue}}/(R_{\text{sourcecapillary}} + R_{\text{sourcetip}} + R_{\text{tissue}} + R_{\text{HBSS}} + R_{\text{collectioncapillary}}) \quad (8)$$

The factor β was found to be 0.144 by forcing eq 8 to equal the central value in Figure 3 (($V_{\text{tissue}}/V_{\text{app}}$) = 8.3×10^{-4} for a 200 μm i.d. source barrel, 20 μm source tip, 75 μm i.d. collection capillary).

Damage Trends. Neither the source tip size nor the insertion depth of the source capillary (DBS) had a significant effect on damage in the range we tested (Figure SI-4, panels A and B). However, as Figure 5 shows, damage in the CA3 is correlated to the voltage drop in the tissue. Although there is considerable scatter in the results, it can also be seen that the CTD had minimal influence on cell death. When the CTD is zero, damage occurs.[40] We suspect that the damage caused in this situation is not electrical. In this COMSOL model, we did not permit the tissue to deform or change shape. In reality,
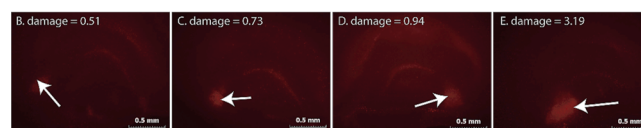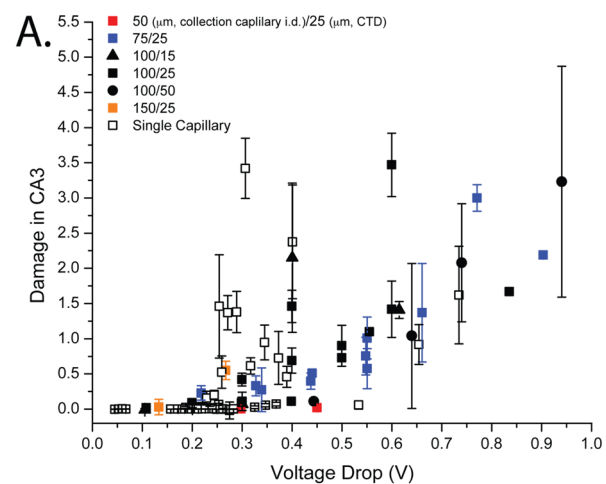
Figure 5. Damage versus the voltage drop within the tissue. (A) Damage in CA3 versus COMSOL-calculated voltage drop for both EOPPP and the single capillary configuration. The numbers indicated in the legend are collection capillary i.d./collection capillary-to-tissue distance. For all points, the source barrel was 200 μm. For EOPPP (solid data points) voltage drop is the difference in voltages between source capillary and tissue surface under the collection capillary. Data for the single capillary sampling are taken from Hamsher et al.[40] For these data, the voltage drop is the difference between the surface and bottom of the tissue. Total n = 170. (B−E) are PI-stained images representing different damage values as indicated on each image. Error bars are SEM, total n (EOPPP) = 151, and total n (single capillary) = 270.

because the tissue and capillary do not have the same zeta potentials[44,45] there is a contribution of pressure to fluid flow between capillaries.[28] When the capillary and tissue are adjacent, the pressure may damage the tissue by pressing it against the capillary. The increased capillary-to-tissue distance at the collection capillary might relieve some pressure on the tissue at this interface, minimizing damage from physical stress.

Damage in the CA1 and DG-IP was also investigated, compared to the CA3, and shown in Figure 6. The CA1 was
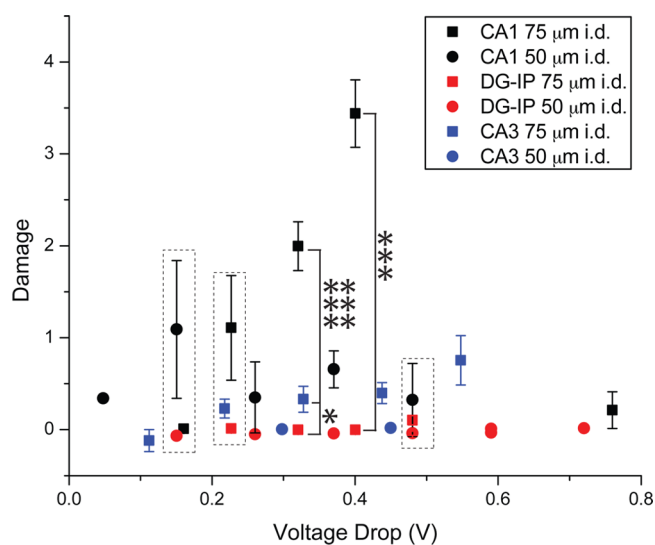
Figure 6. Tissue damage in the CA3, CA1, and DG-IP from electroosmotic sampling in each area. In each case, the source capillary i.d. was 200 μm, the source tip was 25 μm, the DBS was 60 μm and the CTD was 25 μm. The i.d. of the collection capillary was either 50 or 75 μm. The y-axis is damage calculated according to eq 1. Error bars are SEM. Statistical tests were performed on sets of data that were collected under similar voltage drops. Data points marked with asterisks (*) indicate significant difference (*** = $p < 0.005$, * = $p < 0.05$). Those outlined in a dashed line were tested, but differences were not significant.

more vulnerable than the CA3 under identical sampling conditions with the statistical significance shown in Figure 6. The DG-IP is hardly affected at all by the conditions used. Figure 7 addresses damage in EOPPP sampling as a function of power dissipated, illustrating that there was a correlation between damage and power, although results from the single capillary approach and EOPPP are not superimposed (see Figure SI-5 for set plotted on the same graph). The fact that the correlation with power was different for the single- and two-capillary approaches, while the damage correlation with voltage drop in the tissue correlated similarly in both experiments suggests that the voltage itself rather than a manifestation of the voltage, for example, Joule heating, is responsible for the damage.

While the voltage drop or power can be used to estimate damage, it is most practical to summarize trends in terms of actual experimental parameters such as applied voltages and capillary dimensions. In the single capillary design,[38,39] we found that decreasing the collection capillary i.d. and increasing the collection capillary-to-tissue distance minimized the damage associated with sampling.[40] Collection capillary i.d. is still the overarching factor that dictates damage in EOPPP, as insertion depth, tip diameter of the source capillary, and capillary-tissue distance at the dimensions tested, had little influence. We did
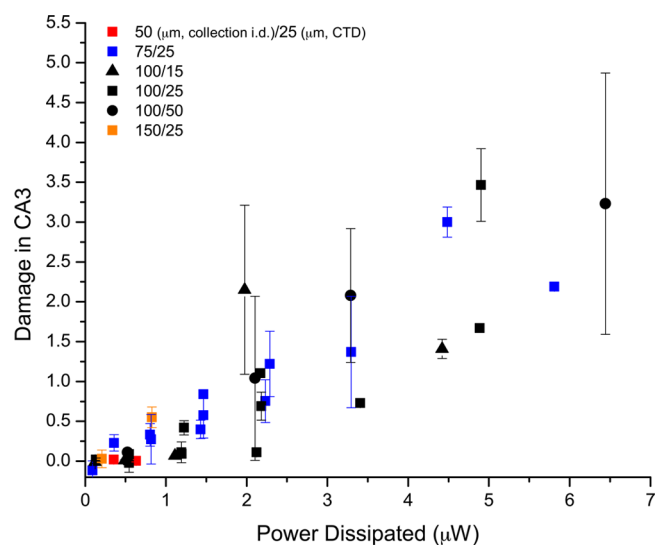
Figure 7. Damage in CA3 with respect to power dissipated in the tissue. Damage in CA3 versus COMSOL-calculated power dissipated for EOPPP. The numbers indicated in the legend are collection capillary i.d./collection capillary-to-tissue distance. For all points, the source barrel was 200 μm. Power was calculated by integrating the square of the electric field over the tissue domain in COMSOL and multiplying by the conductivity of the tissue. Error bars are SEM, total $n = 151$.

not investigate the source capillary barrel diameter. However, based on the model of simple resistance, decreasing a capillary diameter decreased the voltage drop in the tissue. Thus, we predict that a smaller source capillary decreases damage.

An electric field in tissue will affect the transmembrane potential of a cell, but the effects vary depending on the strength of the field, the size and shape of the cell, and length of time that the field is applied. When a cell is depolarized for prolonged periods of time, such as during exposure to high concentrations of potassium, the cell membrane and health of the cell can be compromised.[46] However, prolonged weak DC fields have been used in a variety of beneficial applications, from modulating neuronal excitability in hippocampal slice cultures[47,48] to treating stroke patients through transcranial direct current stimulation.[49] High electric fields can cause electroporation;[50] however, the average fields in the tissue were well below the electroporation threshold.

We turn to COMSOL to infer how the electric field may interact locally with neurons in the tissue. We visualized the electric field outside of the source capillary, noting that the electric field at the tip of the source capillary was rather high but decayed rapidly in every direction outside the tip (except within the capillary itself). The field at a 20 μm radius from the tip is only 10% of that at the tip. At the most, one or two 30 μm pyramidal neurons have a portion of their cell membranes in this zone of high field, but only the portion of the membrane closest to the source capillary will be affected significantly. This side of the cell near the tip will actually be hyperpolarized. The opposite side of the cell, a distance of 30 μm away, will have a less negative transmembrane potential than the resting potential. Because the field is sufficiently decayed at this point, the portion of the cell that *can* be depolarized experiences a much lower field. However, those few cells near the source tip experience the high field for an extended period of time. This may be enough to initiate spreading depression (SD) events.[51] In fact, preliminary but incomplete calcium

853

dx.doi.org/10.1021/cn4000814 | ACS Chem. Neurosci. 2013, 4, 849−857

imaging experiments suggest that over a certain voltage drop threshold, a spreading depression (SD) event could be initiated. These events were more probable when the voltage drop within the tissue was 250 mV or greater, and were not seen at voltage drops less than this value. Despite evidence that spreading depression does not cause damage in normal brain tissue[52] nor in the healthy tissue to which SD waves from an area of damaged tissue may propagate,[53] more extensive experiments are required to understand how the sampling electric field may affect the tissue.

CONCLUSION

We have found correlation between damage to an OHSC sampled by EOPPP and various sampling conditions. In general, conditions leading to low or no observable cell death (based on PI fluorescence) are those that have low dissipated power and low voltage drops between capillaries. This can be achieved by using capillaries with smaller diameters. Neither the size of the source tip nor the source tip insertion depth influenced the overall damage as greatly as the collection capillary i.d.

For a sampling method to be viable, it is important, imperative really, to be aware of how sample collection affects the sample and the information contained within. If possible, one should try to minimize this external influence on the information content in the acquired sample. We can only learn information about endogenous mechanisms when we know that these mechanisms are not changed due to the sampling method itself. This work, combined with the companion paper[54] shows that we are able to realistically sample the extracellular space without causing a great deal of damage. However, the observed trends serve simply to guide an experiment. Individual circumstances will dictate specific parameters. For example, a study of the release of neurotransmitters in the extracellular space requires close attention to preventing cell death and preventing depolarization. However, if one were looking for ectopeptidase activity, as long as the cell membrane remains intact during the experiment, there should be no significant effect of related to cell damage that is only seen several hours after the experiment is over.

In addition to establishing trends with experimental data, we have developed a working correlation through the use of COMSOL simulations between electrical conditions in the tissue and the experimental damage. This correlation can be extended to other conditions and other models to predict impact of sampling conditions on the tissue prior to actual sampling.

METHODS

Solution and Reagents. Tissue culture medium was 50% opti-MEM, 25% horse serum, 25% Hank's balanced salt solution with phenol red (all from Gibco, of Life Technologies, Carlsbad, CA), supplemented with 1% D-(+)-glucose (Sigma-Aldrich, St. Louis, MO), and filtered through a Nalgene filter (0.1 μm pore size, Fisher Scientific, Waltham, MA). Part way through this work, the surgical protocol was modified. The two protocols differ in treatment of freshly chopped tissues. In the initial method of tissue preparation, filtered Gey's balanced salt solution (GBSS, Sigma-Aldrich) supplemented with 0.5% D-(+)-glucose and 2.7 mM MgSO$_4$ was used as the dissection solution. The dissection solution in the altered protocol was a serum-free version of the culture medium, substituting opti-MEM solution for the horse serum. Hank's balanced buffer solution (HBSS, Gibco) was used during sampling, for rinsing of tissues, and for culture imaging. Propidium iodide (PI) solutions for cell death studies were prepared by dissolving solid PI (Sigma-Aldrich) in HBSS at a final concentration of 0.35 mM and freezing until use.

Surgical and Culturing Procedure. Surgical and culturing were done in the same fashion as previously.[54] During the time of data acquisition, the surgical protocol for preparing tissue cultures was altered to obtain healthier tissues that lived longer than those we had been preparing. We will call the first protocol the "initial" protocol.[44] The new technique was that outlined by Gogolla et al.[55] and will be referred to as the Gogolla technique. As only normal, viable cultures were used in experiments, differences in culture survival rate resulting from changing the protocol did not influence the results.

In both protocols, the hippocampal region of a 7 days postnatal (p7) Sprague−Dawley rat pup was removed from the brain and chopped perpendicular to the septotemporal axis using a tissue chopper (McIlwain, model TC752) to a thickness of 350 μm. There were three significant differences between the two surgical protocols: (1) The Gogolla technique called for disinfection of freshly decapitated heads by submersion in 70% ethanol prior to dissection. (2) The dissected hippocampi were transferred to the tissue chopper in a "wet" fashion via submersion in dissection medium and transferred from there with a wide-bore pipet. This contrasts to the initial procedure in which transfer was done in a "dry" fashion by simply placing the dissected hippocampi on the chopper surface with a spatula. (3) The Gogolla protocol involved incubating freshly chopped slices at 4 °C in dissection medium for 30−90 min before plating. Tissue slices that remained attached to others were separable by gently swirling the dish and/or gently aspirating medium and slices with a wide bore pipet. Rarely, slices needed to be carefully pried apart with spatulas. In the initial surgical protocol, freshly chopped tissues were immediately submerged in GBSS (4 °C), physically separated with a microspatula, and immediately plated.

Plating and all culture maintenance following plating were identical in both procedures. To plate, 2−3 tissues were placed onto each porous (0.4 μm) modified PTFE insert membrane surface (Millipore, Bedford, MA), and cultured in a 6-well plate (Sarstedt, Newton, NC) over 1.2 mL of serum-containing medium. The OHSCs were incubated in 5% CO$_2$ and 95% air for 5−8 days at 36.5 °C before use. The medium was exchanged every 2−3 days during incubation.

Sampling: General procedure. To check viability of tissues before use in experiments, PI was added to the culture medium at a final concentration of 7 μM 16−24 h prior to the desired sampling time. To create a positive control for tissue damage, one pair of cultures on a single insert was intentionally killed by direct exposure to 20−50 μL of methanol (MeOH). After 1−2 min of exposure, excess MeOH was then aspirated away. To prepare tissues for imaging, the PI-containing medium was exchanged for warmed (37 °C), PI-free culture medium. PI fluorescence was detected using an inverted fluorescence microscope (IX-71 with U-MGIW2 cube from Olympus, Melville, NY) equipped with a 4× (0.16 NA) objective and image acquisition software (Simple PCI). The exposure time used for assessing PI fluorescence was set to the lowest autoexposure time for the two MeOH-treated OHSCs. Any OHSC showing extensive cell death was noted and not used for sampling. In addition to screening via PI staining, the general structural integrity and proper morphology was examined under bright field. Tissues in which any part of the hippocampal formation was unrecognizable or in which abnormal growth is observed were also discarded. All tissues were then returned to the incubator while preparations were made for sampling, typically begun within the next hour.

Capillary Preparation and Mounting. Both capillaries were made of fused silica (Polymicro Technologies, L.L.C., Phoenix, AZ). The collection capillary, with i.d. varying from 50 to 150 μm, was cut to 30 cm with a Shortix capillary cutter (Scientific Instrument Services, Ringoes, NJ), which uses a diamond blade to ensure a clean, straight cut to the end. The source capillary was prepared by pulling capillaries of 200 μm i.d. fused silica capillary to a bee-stinger-type tip using a capillary puller (model P-2000, Sutter Instruments, Inc., Novato, CA). The bee-stinger tip was trimmed with a razor blade to create the desired tip diameter (15−30 μm). This process was monitored by live imaging on the IX-71 microscope under bright field illumination. The

854

dx.doi.org/10.1021/cn4000814 | ACS Chem. Neurosci. 2013, 4, 849−857

capillaries were mounted on two separate electronic micromanipulators (Model MP-285, Sutter Instruments, Inc.) attached to the IX-71 microscope stage. The electronic manipulators allowed precise control of the sampling and source lumen in and around the tissue surface. The distal end of each capillary was held in place in a dish filled with HBSS. The source capillary was mounted at a 45° angle to the microscope stage and the collection capillary perpendicular to the microscope stage.

Capillary Filling. The collection capillary was filled with HBSS through syringe injection from the proximal end of the capillary. The source capillary was best filled by applying a vacuum to the nontapered distal end while the proximal tapered tip was submerged in the HBSS which was filtered through a filter apparatus containing an inline frit with a 0.5 μm pore size (Idex Health and Science, Oak Harbor, WA). To avoid siphoning, the fluid below the tissue was at the same height as the fluid in the dish at the distal end of the source capillary.

Capillary Positioning. The positions of each capillary were carefully monitored by the shadows the capillaries cast over the tissue when live imaging in bright field mode. Figure SI-7 describes the capillary placement process. The source capillary tip was inserted into the tissue at a desired insertion depth (referred to as DBS in several instances within this publication) and the collection capillary positioned above the tissue, in contact with HBSS solution, at a desired distance (CTD). The distance between the capillaries could be calculated geometrically, according to the diagram illustrated in Figure SI-3.

Platinum electrodes attached each proximal HBSS-filled dish to a high voltage source, model PS350 from Stanford Research Systems (Sunnyvale, CA). Once the capillaries are positioned, the voltage source was turned on and sampling commenced.

One 6-well plate was removed at a time from the incubator for all sampling experiments. All viable OHSCs were sampled before the plate was returned to the incubator, remaining out for approximately 1.5 h. In any given 6-well plate, at least two tissues were not sampled to serve as live (negative) controls. Capillary-to-tissue distances ranged from 15 to 50 μm and source insertion depths were either 40 or 60 μm. With these parameters, the distance between the center of the source lumen to the tissue surface under the center of the sampling lumen ranged from 100 to 150 μm. Applied voltage ranged from 100 to 800 V and was applied for 5 min. After sampling one location in a tissue, the voltage was shut off and the capillaries were removed and sampling proceeded to the next tissue. After sampling all the desired tissues, all negative controls (two per plate), two positive controls (MeOH-treated), and all sampled tissue were treated with PI (7 μM in culture medium) overnight. The next day, medium was exchanged for HBSS buffer solution for imaging. Imaging was done in the same fashion as the screening for cell death prior to sampling, using the IX-71 inverted fluorescence microscope with a 4× objective, setting the exposure time to the lowest of the auto exposure times of the two MeOH-treated tissues.

ASSOCIATED CONTENT

ⓢ Supporting Information

COMSOL model parameters; geometry of capillary placement; effect of source tip size and insertion depth on damage; relationship of damage to power for one- and two-capillary sampling; diagram of experimental setup; bright field images of the capillary positioning procedure. This material is available free of charge via the Internet at http://pubs.acs.org.

AUTHOR INFORMATION

Corresponding Author
*E-mail: sweber@pitt.edu.

Author Contributions
S.G.W. and A.E.R. designed experiments. A.E.R. carried out all experiments. A.E.R. and Y.O. performed numerical simulations. A.E.R., S.G.W. wrote the manuscript and Y.O. designed the table of contents graphic. M.S. served as a consultant on PI and on effects of electric fields on hippocampal neurons.

Notes
The authors declare no competing financial interest.

■ REFERENCES

(1) Elliott-Hunt, C., Marsh, B., Bacon, A., Pope, R., Vanderplank, P., and Wynick, D. (2004) Galanin acts as a neuroprotective factor to the hippocampus. *Proc. Natl. Acad. Sci. U.S.A. 101*, 5105−5110.

(2) Zini, S., Roisin, M., Langel, U., Bartfai, T., and Ben-Ari, Y. (1993) Galanin reduces release of endogenous excitatory amino acids in the rat hippocampus. *Eur. J. Pharmacol. Mol. Pharmacol. 245*, 1−7.

(3) Zini, S., Roisin, M., Armengaud, C., and Ben-Ari, Y. (1993) Effect of potassium channel modulators on the release of glutamate induced by ischemic-like conditions in rat hippocampal slices. *Neurosci. Lett. 153*, 202−205.

(4) Reiss, J. I., Dishman, R. K., Boyd, H. E., Robinson, J. K., and Holmes, P. V. (2009) Chronic activity wheel running reduces the severity of kainic acid-induced seizures in the rat: possible role of galanin. *Brain Res. 1266*, 54−63.

(5) Mazarati, A., Hohmann, J., Bacon, A., Liu, H., Sankar, R., Steiner, R., Wynick, D., and Wasterlain, C. (2000) Modulation of hippocampal excitability and seizures by galanin. *J. Neurosci. 20*, 6276−6281.

(6) Mazarati, A., Liu, H., Soomets, U., Sankar, R., Shin, D., Katsumori, H., Langel, U., and Wasterlain, C. (1998) Galanin modulation of seizures and seizure modulation of hippocampal galanin in animal models of status epilepticus. *J. Neurosci. 18*, 10070−10077.

(7) Hwang, I., Yoo, K.-Y., Kim, D., Do, S.-G., Oh, Y.-S., Kang, T.-C., Han, B., Kim, J., and Won, M. (2004) Expression and changes of galanin in neurons and microglia in the hippocampus after transient forebrain ischemia in gerbils. *Brain Res. 1023*, 193−199.

(8) de Gortari, P., Romero, F., Cisneros, M., and Joseph-Bravo, P. (2005) Acute administration of alcohol modulates pyroglutamyl amino peptidase II activity and mRNA levels in rat limbic regions. *Neurochem. Int. 46*, 347−356.

(9) Irazusta, J., Larrinaga, G., Agirregoitia, N., Varona, A., and Casis, L. (2003) Effects of morphine administration and its withdrawal on rat brain aminopeptidase activities. *Regul. Pept. 110*, 225−230.

(10) Irazusta, J., Tejedor-Real, P., Varona, A., Costela, C., Gilbert-Rahola, J., and Casis, L. (1999) Effect of neonatal handling on brain enkephalin-degrading peptidase activities. *Neurochem. Int. 35*, 357−361.

(11) Bedecs, K., Langel, U., and Bartfai, T. (1995) Metabolism of galanin and galanin (1−16) in isolated cerebrospinal fluid and spinal cord membranes from rat. *Neuropeptides 29*, 137−143.

(12) Ogawa, T., Kiryu-Seo, S., Tanaka, M., Konishi, H., Iwata, N., Saido, T., Watanabe, Y., and Kiyama, H. (2005) Altered expression of neprilysin family members in the pituitary gland of sleep-disturbed rats, an animal model of severe fatigue. *J. Neurochem. 95*, 1156−1166.

(13) Freed, A. L., Audus, K. L., and Lunte, S. M. (2001) Investigation of the metabolism of substance P at the blood-brain barrier using capillary electrophoresis with laser-induced fluorescence detection. *Electrophoresis 22*, 3778−3784.

(14) Westerink, B. (1992) Monitoring molecules in the conscious brain by microdialysis. *TrAC, Trends Anal. Chem. 11*, 176−182.

(15) Baines, C., Kaiser, R., Purcell, N., Blair, N., Osinska, H., Hambleton, M., Brunskill, E., Sayen, M., Gottlieb, R., Dorn, G., Robbins, J., and Molkentin, J. (2005) Loss of cyclophilin D reveals a critical role for mitochondrial permeability transition in cell death. *Nature 434*, 658−662.

(16) Yin, K. J., Cirrito, J. R., Yan, P., Hu, X., Xiao, Q., Pan, X., Bateman, R., Song, H., Hsu, F. F., Turk, J., Xu, J., Hsu, C. Y., Mills, J. C., Holtzman, D. M., and Lee, J. M. (2006) Matrix metalloproteinases

expressed by astrocytes mediate extracellular amyloid-beta peptide catabolism. *J. Neurosci.* 26, 10939−10948.

(17) Zhang, H., Stoeckli, M., Andren, P. E., and Caprioli, R. M. (1999) Combining solid-phase preconcentration, capillary electrophoresis and off-line matrix-assisted laser desorption/ionization mass spectrometry: intracerebral metabolic processing of peptide E in vivo. *J. Mass Spectrom.* 34, 377−383.

(18) Cirrito, J. R., May, P. C., O'Dell, M. A., Taylor, J. W., Parsadanian, M., Cramer, J. W., Audia, J. E., Nissen, J. S., Bales, K. R., Paul, S. M., DeMattos, R. B., and Holtzman, D. M. (2003) In vivo assessment of brain interstitial fluid with microdialysis reveals plaque-associated changes in amyloid-beta metabolism and half-life. *J. Neurosci.* 23, 8844−8853.

(19) Sanderson, K., Andren, P. E., Caprioli, R. M., and Nyberg, F. (1996) In vitro metabolism of LVV-hemorphin-7 in human plasma studied by reversed-phase high-performance liquid chromatography and micro-electrospray mass spectrometry. *J. Chromatogr., A* 743, 207−212.

(20) Eriksson, U., Andren, P. E., Caprioli, R. M., and Nyberg, F. (1996) Reversed-phase high-performance liquid chromatography combined with tandem mass spectrometry in studies of a substance P-converting enzyme from human cerebrospinal fluid. *J. Chromatogr., A* 743, 213−220.

(21) Andren, P. E., and Caprioli, R. M. (1995) In vivo metabolism of substance P in rat striatum utilizing microdialysis/liquid chromatography/micro-electrospray mass spectrometry. *J. Mass Spec.* 30, 817−824.

(22) Nydahl, K. S., Pierson, J., Nyberg, F., Caprioli, R. M., and Andren, P. E. (2003) In vivo processing of LVV-hemorphin-7 in rat brain and blood utilizing microdialysis combined with electrospray mass spectrometry. *Rapid Commun. Mass Spectrom.* 17, 838−844.

(23) Kottegoda, S., Shaik, I., and Shippy Scott, A. (2002) Demonstration of low flow push-pull perfusion. *J. Neurosci. Methods* 121, 93−101.

(24) Slaney, T. R., Nie, J., Hershey, N. D., Thwar, P. K., Linderman, J., Burns, M. A., and Kennedy, R. T. (2011) Push-pull perfusion sampling with segmented flow for high temporal and spatial resolution in vivo chemical monitoring. *Anal. Chem.* 83, 5207−5213.

(25) Pritchett, J., Pulido, J., and Shippy, S. (2008) Measurement of Region-Specific Nitrate Levels of the Posterior Chamber of the Rat Eye Using Low-Flow Push-Pull Perfusion. *Anal. Chem.* 80, 5342−5349.

(26) Kennedy, R. T., Thompson, J. E., and Vickroy, T. W. (2002) In vivo monitoring of amino acids by direct sampling of brain extracellular fluid at ultralow flow rates and capillary electrophoresis. *J. Neurosci. Methods* 114, 39−49.

(27) Kottegoda, S., Pulido, J., Thongkhao-on, K., and Shippy, S. (2007) Demonstration and use of nanoliter sampling of in vivo rat vitreous and vitreoretinal interface. *Mol. Vision* 13, 2073−2082.

(28) Rathore, A. S., and Horvath, C. (1998) Axial nonuniformities and flow in columns for capillary electrochromatography. *Anal. Chem.* 70, 3069−3077.

(29) Delgado, J., DeFeudis, F., Roth, R., Ryugo, D., and Mitruka, B. (1972) Dialytrode for long term intracerebral perfusion in awake monkeys. *Arch. Int. Pharmacodyn. Ther.* 198, 9−21.

(30) Delgado, J., Lerma, J., Martin del Rio, R., and Solis, J. (1984) Dialytrode technology and local profiles of amino acids in the awake cat brain. *J. Neurochem.* 42, 1218−1228.

(31) Redgrave, P. (1977) A modified push-pull system for the localised perfusion of brain tissue. *Pharmacol., Biochem. Behav.* 6, 471−474.

(32) Chefer, V. I., Thompson, A. C., Zapata, A., and Shippenberg, T. S. (2009) Overview of brain microdialysis. *Current Protocols in Neuroscience*, Chapter 7, Unit 7 1, John Wiley & Sons, Inc.: Hoboken, NJ.

(33) Jaquins-Gerstl, A., Shu, Z., Zhang, J., Liu, Y., Weber, S. G., and Michael, A. C. (2011) Effect of Dexamethasone on Gliosis, Ischemia, and Dopamine Extraction during Microdialysis Sampling in Brain Tissue. *Anal. Chem.* 83, 7662−7667.

(34) Jaquins-Gerstl, A., and Michael, A. C. (2009) Comparison of the brain penetration injury associated with microdialysis and voltammetry. *J. Neurosci. Methods* 183, 127−135.

(35) Wang, Y., and Michael, A. C. (2012) Microdialysis probes alter presynaptic regulation of dopamine terminals in rat striatum. *J. Neurosci. Methods* 208, 34−39.

(36) Matala, C., Wang, Y., Borland, L. M., Jung, M., Shand, S., Watkins, S., Weber, S. G., and Michael, A. C. (2008) Impact of microdialysis probes on vasculature and dopamine in the rat striatum: a combined fluorescence and voltammetric study. *J. Neurosci. Methods* 174, 177−185.

(37) Noraberg, J., Kristensen, B., and Zimmer, J. (1999) Markers for neuronal degeneration in organotypic slice cultures. *Brain Res. Protoc.* 3, 278−290.

(38) Xu, H., Guy, Y., Hamsher, A., Shi, G., Sandberg, M., and Weber, S. (2010) Electroosmotic sampling. Application to determination of ectopeptidase activity in organotypic hippocampal slice cultures. *Anal. Chem.* 82, 6377−6383.

(39) Wu, J., Xu, K., Landers, J. P., and Weber, S. G. (2013) An in situ measurement of extracellular cysteamine, homocysteine, and cysteine concentrations in organotypic hippocampal slice cultures by integration of electroosmotic sampling and microfluidic analysis. *Anal. Chem.* 85, 3095−3103.

(40) Hamsher, A., Xu, H., Guy, Y., Sandberg, M., and Weber, S. (2010) Minimizing tissue damage in electroosmotic sampling. *Anal. Chem.* 82, 6370−6376.

(41) Kilb, W., Dierkes, P. W., Sykova, E., Vargova, L., and Luhmann, H. J. (2006) Hypoosmolar conditions reduce extracellular volume fraction and enhance epileptiform activity in the CA3 region of the immature rat hippocampus. *J. Neurosci. Res.* 84, 119−129.

(42) Suman, R., and Ruth, D. (1993) Formation factor and tortuosity of homogeneous porous media. *Transp. Porous Media 12* 12, 185−206.

(43) Sen, P. N. (2007) *J. Phys.: Condens. Matter* 16, S5213−S5220.

(44) Guy, Y., Sandberg, M., and Weber, S. (2008) Determination of ζ-potential in rat organotypic hippocampal cultures. *Biophys. J.* 94, 4561−4569.

(45) Guy, Y., Muha, R., Sandberg, M., and Weber, S. (2009) Determination of ζ-potential and tortuosity in rat organotypic hippocampal cultures from electroosmotic velocity measurements under feedback control. *Anal. Chem.* 81, 3001−3007.

(46) Takahashi, M., Liou, S.-Y., and Kunihara, M. (1995) Ca^{2+}- and Cl^--dependent, NMDA receptor-mediated neuronal death induced by depolarization in rat hippocampal organotypic cultures. *Brain Res.* 675, 249−256.

(47) Gluckman, B., Neel, E., and Netoff, T. (1996) Electric field suppression of epileptiform activity in hippocampal slices. *Mol. Cell. Biochem.* 76, 4202−4205.

(48) Bikson, M., Inoue, M., Akiyama, H., Deans, J., Fox, J., Miyaka, H., and Jefferys, J. (2004) Effects of uniform extracellular DC electric fields on excitability in rat hippocampal slices in vitro. *J. Physiol. (Oxford, U. K.)* 557, 175−190.

(49) Datta, A., Baker, J. M., Bikson, M., and Fridriksson, J. (2011) Individualized model predicts brain current flow during transcranial direct-current stimulation treatment in responsive stroke patient. *Brain Stimul.* 4, 169−174.

(50) Nolkrantz, K., Farre, C., Brederlau, A., Karlsson, R., Brennan, C., Eriksson, P., Weber, S., Sandberg, M., and Orwar, O. (2001) Electroporation of single cells and tissues with an electrolyte-filled capillary. *Anal. Chem.* 73, 4469−4477.

(51) Snow, R. W., Taylor, C. P., and Dudek, F. E. (1983) Electrophysiological and optical changes in slices of rat hippocampus during spreading depression. *J. Neurophysiol.* 50, 561−572.

(52) Nedergaard, M., and Hansen, A. J. (1988) Spreading depression is not associated with neuronal injury in the normal brain. *Brain Res.* 449, 395−398.

(53) Oliveira-Ferreira, A. I., Milakara, D., Alam, M., Jorks, D., Major, S., Hartings, J. A., Luckl, J., Martus, P., Graf, R., Dohmen, C., Bohner, G., Woitzik, J., and Dreier, J. P. (2010) Experimental and preliminary clinical evidence of an ischemic zone with prolonged negative DC

shifts surrounded by a normally perfused tissue belt with persistent electrocorticographic depression. *J. Cereb. Blood Flow Metab. 30,* 1504−1519.

(54) Rupert, A. E., Ou, Y., Sandberg, M., and Weber, S. G. (2013) Electroosmotic push-pull perfusion: description and application to qualitative analysis of the hydrolysis of exogenous galanin in organotypic hippocampal slice cultures. *ACS Chem. Neurosci.* DOI: 10.1021/cn400082d.

(55) Gogolla, N., Galimberti, I., DePaola, V., and Caroni, P. (2006) Preparation of organotypic hippocampal slice cultures for long-term live imaging. *Nat. Protoc. 1,* 1165−1171.